Journal of Power Sources 193 (2009) 408–415

Contents lists available at ScienceDirect

Journal of Power Sources

journal homepage: www.elsevier.com/locate/jpowsour

Promoting effect of CeO_2 in the electrocatalytic activity of rhodium for ethanol electro-oxidation

Q. He [a], S. Mukerjee [a], B. Shyam [b], D. Ramaker [b], S. Parres-Esclapez [c], M.J. Illán-Gómez [c], A. Bueno-López [c,*]

[a] Department of Chemistry & Chemical Biology, Northeastern University, 360 Huntington Ave, Boston, 02115 MA USA
[b] Department of Chemistry, George Washington University, 725 21st Street N.W, Washington, DC 20052, USA
[c] Department of Inorganic Chemistry, University of Alicante, Ap. 99 E-03080, Alicante, Spain

ARTICLE INFO

Article history:
Received 15 December 2008
Received in revised form 4 March 2009
Accepted 25 March 2009
Available online 5 April 2009

Keywords:
Ethanol electro-oxidation
Electrocatalyst
Ceria
Rhodium
DAFC
DEFC

ABSTRACT

The promoting effect of ceria in the electrocatalytic activity of rhodium for ethanol electro-oxidation in alkali media has been studied. Rh/C, CeO_2/C and $RhCeO_2$/C catalysts were synthesized and characterized by TEM, XRD, XPS, TG-MS, H_2-TPR and XAS. The electrocatalytic activity was studied by Cyclic Voltammetry (CV) and chronoamperometry. The onset potential of oxidation on $RhCeO_2$/C was shifted negatively as compared to that on Rh/C, despite ceria itself does not show any electrocatalytic activity. The promoting effect of ceria has been attributed to the improved rhodium dispersion, and differences in the oxidation state of rhodium between Rh/C and $RhCeO_2$/C were not found. The carbon support reduces rhodium species to Rh^0, and also partially reduces ceria, during the samples preparation, and the surface of the carbon support is oxidised.

1. Introduction

The Direct Alcohol Fuel Cell (DAFC) is a promising technology for transportation and portable electronic devices, and ethanol seems to be preferred to methanol for DAFCs because has higher energy density, is safer, and can be produced in great quantities from biomass [1,2].

Carbon supported platinum is commonly used as anode catalyst in low temperature fuel cells. However, pure platinum is not the most efficient anodic catalyst since it is rapidly poisoned by strongly adsorbed species coming from the dissociative adsorption of ethanol [1,2]. As a big breakthrough in the development of catalysts for electro-oxidation of ethanol, $PtRhSnO_2$/C was synthesized recently by depositing Pt and Rh atoms on Sn oxides nanoparticles [3]. It has shown strong capability to accomplish C–C bond breaking and significantly better catalytic activity than Pt/C and $PtSnO_2$/C catalysts. In fact, Rh shows high ability to facilitate the C–C bond cleavage due to interaction of ethanol molecule with the Rh metallic surface and formation of cyclic adsorbate [4,5]. However, not only full dehydrogenation and C–C bond dissociation but also consequent formation and oxidation of adsorbed carbon monoxide on catalyst surface were involved during the process of electro-oxidation of ethanol. It may not be sufficient to overcome high activation energy and CO poison by using Rh alone [6]. Generally, the overall reaction rate of Rh for ethanol oxidation is not comparable with that of Pt and Pt-based alloy [6,7]. Palladium catalysts have been also proposed for this application, and it has been found that the catalytic activity of platinum and palladium-based catalysts for ethanol or methanol oxidation can be enhanced with addition of certain metal oxides in a high pH environment [8–12]. Mann et al. [13] developed PtSnO and PtSnInO catalysts offering partial conversion of ethanol to its 12-electron oxidation products. The mechanism for the promotion effect of oxide proposed was that the electron affinity of tin oxide on a Pt surface is sufficient to pull the methyl group off the carbon of a surface-bound ethanol [13]. Oxide (CeO_2, NiO, Co_3O_4 and Mn_3O_4)-promoted Pd/C electrocatalysts for alcohol electro-oxidation were also fully studied in alkaline media [14]. The authors found that there is an optimum ratio for oxide and Pd and analogized the effect of oxide with RuO_2 in a PtRu alloy catalyst. Nevertheless, the exact role of oxide to promote the activity of noble metal towards electro-oxidation of small molecule alcohols is still unknown.

The promoting effect of metal oxides in the electrocatalytic activity of other noble metals like rhodium has not been reported. However, the promoting effect of CeO_2-based materials in the catalytic activity of rhodium, and other platinum group metals (PGM), for some other chemical reactions is very well known. The best example is found in the three-way catalysts (TWC) used in gasoline vehicles for the simultaneous removal of NO_x, hydrocarbons and CO [15–17]. CeO_2-based mixed oxides represented an important

* Corresponding author. Tel.: +34 965 90 34 00x2226; fax: +34 965 90 34 54.
E-mail address: agus@ua.es (A. Bueno-López).

0378-7753/$ – see front matter © 2009 Elsevier B.V. All rights reserved.
doi:10.1016/j.jpowsour.2009.03.056

improvement of the TWC technology since the early 1980s, and multiple effects have been attributed to this promoter. Ceria was suggested to promote the noble metal dispersion, increase the thermal stability of the Al_2O_3 support, promote the water gas shift (WGS) and steam reforming reactions, favors catalytic activity at the interfacial metal–support sites, promote CO removal through oxidation employing a lattice oxygen and store and release oxygen under lean and rich conditions respectively [15].

The aim of this paper is to study the promoting effect of ceria in the electrocatalytic activity of rhodium for ethanol electrooxidation in alkali media. Rh/C, CeO_2/C and $RhCeO_2$/C catalysts were synthesized in-house and characterized by transmission electron microscopy (TEM), X-ray diffraction (XRD), X-ray photoelectron spectroscopy (XPS), thermo-gravimetry coupled to mass spectroscopy (TG-MS), temperature-programmed reduction (H_2-TPR) and X-ray absorption spectroscopy (XAS). The electrocatalytic activity was studied by Cyclic Voltammetry (CV), and better performance of $RhCeO_2$/C in comparison to Rh/C was observed. The role of CeO_2 in enhancing the catalytic activity of rhodium is discussed on the basis of the characterization and electrocatalytic activity results.

2. Experiment

2.1. Preparation of catalyst powders

The powder samples prepared are denoted by Rh/C, CeO_2/C and $RhCeO_2$/C. A carbon black (C) from Cabot (Vulcan XC72) was used as carbon support, and the rhodium and cerium precursors used were $Rh(NO_3)_3$ and $Ce(NO_3)_3{\cdot}6H_2O$, respectively, both from Aldrich. The samples were prepared as follows:

- Rh/C: The carbon support was impregnated with a water–ethanol solution of the rhodium precursor (80 ml g^{-1}_{carbon}; vol. ratio water:ethanol = 1:1), dried and heat-treated.
- CeO_2/C: The carbon support was impregnated with a water–ethanol solution of the cerium precursor (80 ml g^{-1}_{carbon}; vol. ratio water:ethanol = 1:1), and a water solution of NH_3 (30%) was dropped until pH = 9. The sample was dried and heat-treated.
- $RhCeO_2$/C: The sample CeO_2/C was impregnated with a water–ethanol solution of the rhodium precursor (80 ml g^{-1}_{carbon}; vol. ratio water:ethanol = 1:1), dried and heat-treated.

The drying steps were carried out at 110 °C in static air for 12 h, and the heat-treatments were performed at 500 °C for 2 h under N_2 flow. The concentrations of the different solutions were selected to reach 10 wt% cerium and/or 10 wt% rhodium in the rhodium-containing samples.

2.2. Characterization of catalyst powders

X-ray diffractograms of the catalyst powders were recorded in a Rigaku diffractometer, using Cu Kα radiation (λ = 0.15418 nm).

A JOEL (JEM-2010) microscope was used to obtain TEM images. The microscope is equipped with an EDS analyser (Oxford), model INCA Energy TEM100.

XPS characterisation of powder catalysts was carried out in a VG-Microtech Multilab electron spectrometer using Mg Kα (1253.6 eV) radiation source. To obtain the XPS spectra, the pressure of the analysis chamber was maintained at 5×10^{-10} mbar. The binding energy (B.E.) and the kinetic energy (K.E.) scales were adjusted by setting the C1s transition at 284.6 eV, and B.E. and K.E. values were determined with the software Peak-fit of the spectrometer.

A thermobalance coupled to a mass spectrometer (TG-MS set-up) has been used to characterise the powder samples. The TG is form TA Instruments (model SDT 2960) and the MS from Balzers Instruments (model GSD 300 T3). 5 mg of sample was heated in 100 ml min^{-1} Helium flow at 10 °C min^{-1} from 25 to 850 °C.

Temperature programmed reduction with H_2 (H_2-TPR) was carried out in a Micromeritics Pulse ChemiSorb 2705 device, consisting of a tubular quartz reactor (inner diameter 5 mm) coupled to a TCD analyser for H_2 consumption monitoring. The experiments were conducted with 20 mg of powder catalyst heated at 10 °C min^{-1} from 25 to 850 °C in 30 ml min^{-1} flow of 5 vol.% H_2/Ar. A CuO reference sample, supplied by Micromeritics, has been used to quantify H_2 consumption.

XAS measurements were made at beamline X-11 A, National Synchrotron Light Source, Brookhaven National Lab with the Si (1 1 1) monochromator detuned by 40% in order to reject the higher harmonics from the beam. Data were collected in transmission mode using gas ionization detectors (I_0, I_t and I_{ref}). The samples were placed between I_0 and I_t while the 25 μm rhodium foil was placed between I_t and I_{ref}. The IFEFFIT suite (version 1.2.8) was utilized for data processing and analysis. A k-range of 2.748–15.00 $Å^{-1}$ and a Hanning window of 1.14–3.00 Å were used for the fits of both samples. A k-weight of 2 was employed for all the fits. XAS reference scans were carefully calibrated to the edge energy (23,220 eV, Rh-K edge) and aligned to one standard reference scan. Any edge shift corrections applied to the reference foils were also applied to their respective sample scans. A post-edge normalization procedure was then applied to normalize all scans between 0 and 1.

2.3. Electrode preparation and electrochemical measurements

The electrochemical measurements were conducted in a standard three- compartment electrochemical cell at room temperature using a rotating disk electrode (RDE) setup from Pine Instruments connected to an Autolab (Ecochemie Inc. Model-PGSTAT 30). A glassy carbon disk with 5 mm diameter was used as the substrate for deposition of catalyst films. Before deposition of catalyst films, the RDE was first polished with 0.05 μm alumina slurry (Buehler, Lake Bluff, IL) and then cleaned with distilled water under sonication. All electrochemical experiments were carried out at room temperature (25 °C).

The catalyst inks were prepared by dispersion of certain amounts of catalyst powders into 20 ml of isopropanol and then sonicated for at least 30 min to reach a uniform suspension. The catalyst film was prepared by dispersing 8 μL of the catalyst ink on the glassy carbon (GC) substrate and dried at room temperature to reach a total catalyst loading of 75 μg cm^{-2}. CVs and CAs were taken in 1.0 mol L^{-1} KOH while a Hg/HgO (KOH 1.0 mol L^{-1}) electrode was used as reference electrode.

3. Results and discussion

3.1. Electrochemical measurements

Fig. 1 shows CV curves of Rh/C and $RhCeO_2$/C catalysts in 1 M KOH. The hump at 0.7 V on CV of Rh/C is presumed to be from oxidation of rhodium metal. Ceria shifts this hump to 0.6 V for $RhCeO_2$/C, and in this case, the partial oxidation of both rhodium and ceria could occur. As it will be demonstrated later, rhodium in the original samples is reduced and cerium in the $RhCeO_2$/C sample is only partially oxidized. The negative current observed during the negative scan, mainly in the hydrogen adsorption–desorption region is high, and such current suggests a reduction process, probably reduction of oxygen. Such phenomenon, which is also detected in Figs. 2 and 3, is often observed in alkaline medium when the electrolyte contains some traces of diluted oxygen. However, we are more inclined to believe that such big cathodic current is pertinent to reduction of cerium oxides ($Ce^{4+} \rightarrow Ce^{3+}$), thin film of oxides on

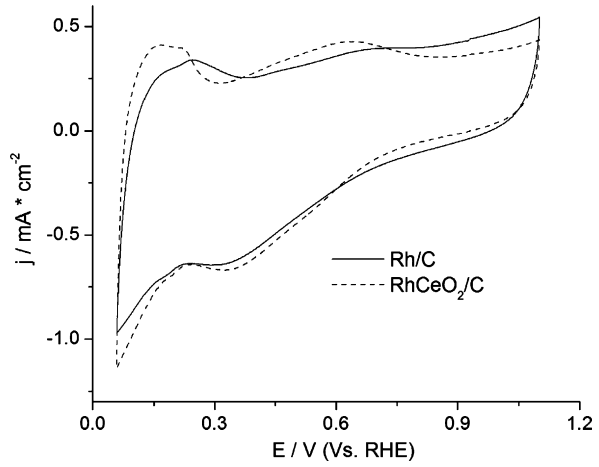

Fig. 1. Cyclic voltammograms for glassy carbon electrodes modified by Rh/C (10 wt% Rh) and $RhCeO_2$/C (10 wt% Rh, 10 wt% Ce) in 1 M KOH. Catalyst loading: 75 μg cm^{-2}, sweep rate 50 mV s^{-1}.

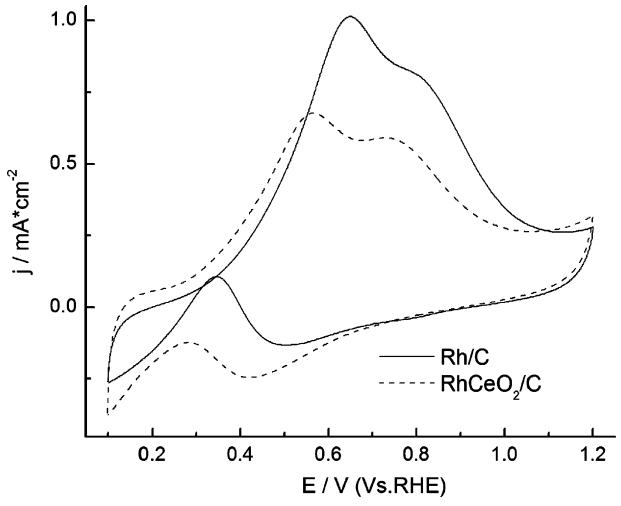

Fig. 2. Cyclic voltammograms for glassy carbon electrodes modified by Rh/C (10 wt% Rh) and $RhCeO_2$/C (10 wt% Rh, 10 wt% Ce) in 1 M KOH + 1 M ethanol. Catalyst loading: 75 μg cm^{-2}, sweep rate 10 mV s^{-1}.

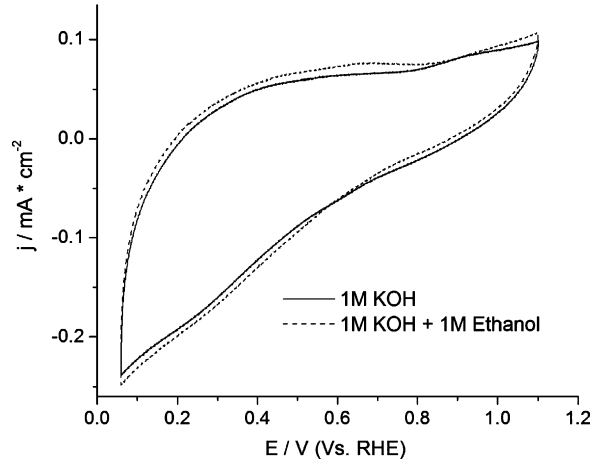

Fig. 3. Cyclic voltammograms for glassy carbon electrodes modified by CeO_2/C (10 wt% Ce) in 1 M KOH and 1 M KOH + 1 M ethanol. Catalyst loading: 75 μg cm^{-2}, sweep rate: 50 mV s^{-1}.

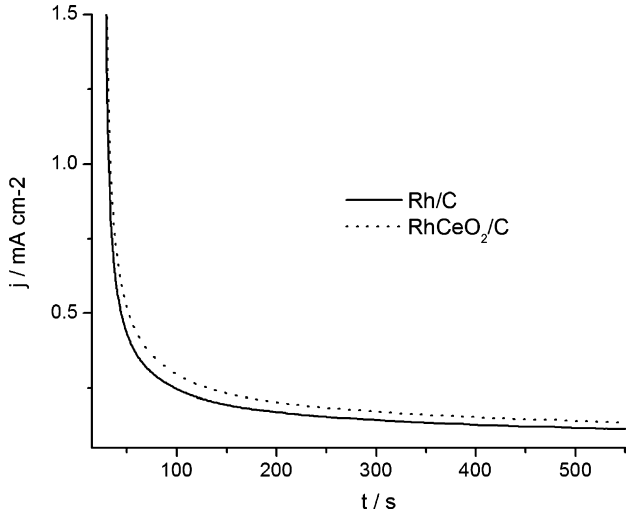

Fig. 4. Chronoamperometric profiles of Rh/C (10 wt% Rh) and $RhCeO_2$/C (10 wt% Rh, 10 wt% Ce) at +0.55 V (vs. RHE) in 1 M KOH + 1 M ethanol. Catalyst loading: 75 μg cm^{-2}.

Rh ($Rh^{\delta+} \rightarrow Rh$) and even surface groups formed on carbon support during the anodic scan [18].

Fig. 2 shows CV curves of ethanol electro-oxidation on Rh/C and $RhCeO_2$/C catalysts. For comparison, CVs of CeO_2/C with and without ethanol in solution were also shown in Fig. 3. Active sites are believed to be located only on rhodium since CeO_2 itself does not show any catalytic activity towards oxidation of ethanol. During the process of electro-oxidation of ethanol on Pt, ethanol decomposes on catalyst surface at low potential and form intermediates such as acetic acid, acetaldehyde and CO [19]. The main products may not to be the same in the case of Rh since we can see one oxidation peak along with a shoulder for both Rh/C and $RhCeO_2$/C, which also appeared in the CVs of Pt/Rh/Pt bilayer [20]. Actually, it was reported by Souza et al. [7] and Vesselli et al. [21] that Rh presents excellent selectivity for complete conversion of ethanol to CO_2 as mentioned during the study in gas phase condition and electrochemical environment [7,21]. In Souza et al.'s [7] study of electro-oxidation of ethanol on Pt, Rh, and PtRh electrodes, the ratio of CO_2 over the acetaldehyde signals increases from pure platinum to pure rhodium electrodes, illustrating that addition of rhodium to platinum electrodes improves the selectivity toward complete electrochemical oxidation of ethanol to CO_2. The anodic current increases due to oxidation of intermediates from decomposition of ethanol as potential goes positively and then decreases after peak potential due to loss of rhodium active sites for the adsorption of intermediates on account of oxygen adsorption [22]. As it has been illustrated in the authors' previous paper [23], the on-set potential is an important parameter to evaluate the activity of catalysts during the electro-oxidation process. The onset potential of oxidation on $RhCeO_2$/C was shifted negatively as much as 35 mV as compared to that on Rh/C, indicating better activity of the former catalyst.

The stability of as-synthesized catalysts was tested by chronoamperometric measurement at 0.55 V (vs. RHE) in Fig. 4. It can be found that the current density decreases quickly and reaches the steady state within 10 min on both Rh/C and $RhCeO_2$/C catalysts. The fact that current on $RhCeO_2$/C diminishes more slowly manifests that CeO_2 helps to reduce accumulation and poisoning of species after ethanol dissociative adsorption [24]. A number of studies on electro-oxidation of alcohols have claimed that easier access of alcohol to active sites of catalysts stems from better dispersion of catalysts nanoparticles [25–28]. Similarly, the well-dispersed $RhCeO_2$/C catalyst pertinent to promoting effect of CeO_2

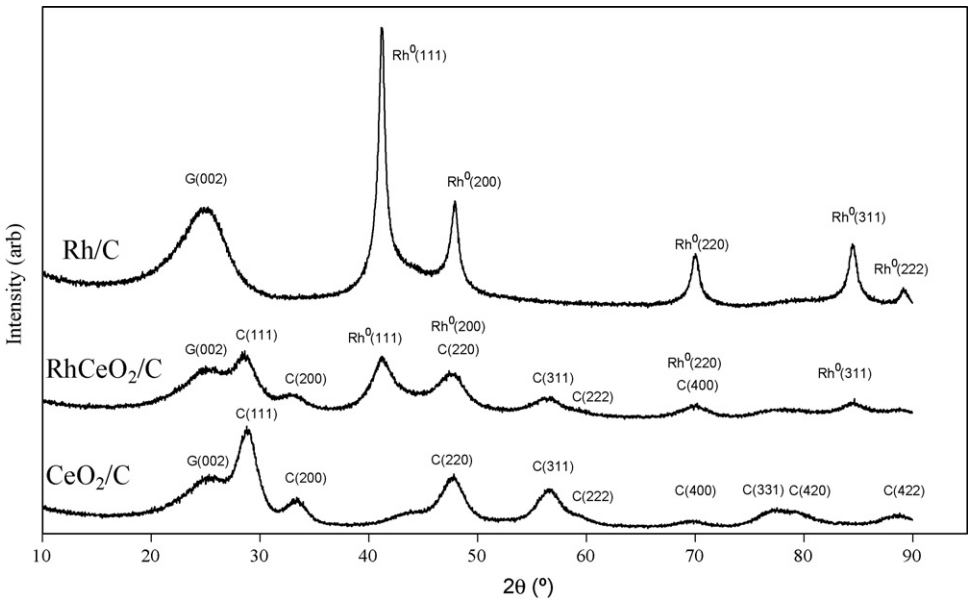

Fig. 5. XRD patterns of the catalyst powders. (C = ceria; G = graphite; Rh^0 = metal rhodium).

response to higher activity and stability towards ethanol oxidation, the salient proofs of which are discussed hereafter.

3.2. Characterization results

In order to analyze the positive effect of CeO_2 in the electrocatalytic activity of rhodium for ethanol electro-oxidation, several characterization techniques have been used, and the results obtained are presented and discussed in this section.

3.2.1. XRD

The X-ray diffractograms of the powder catalysts are shown in Fig. 5, and all the peaks on the three patterns can be attributed to graphite (G), ceria (C) and/or metal rhodium (Rh^0). X-ray diffraction patterns confirm that the cerium-containing catalysts present the main reflections of a fluorite-structured material with a face-centered cubic (fcc) unit cell, corresponding to the (1 1 1), (2 0 0), (2 2 0), (3 1 1), (2 2 2), (4 0 0), (3 3 1), (4 2 0), and (4 2 2) planes [28,29]. The shoulder of the fluorite peak (1 1 1) at low angle is the main graphite peak corresponding to the (0 0 2) plane [30], and is produced by the well-structured carbon black support. This graphite peak is present in the pattern of the three samples tested, as expected. The XRD patterns of the samples Rh/C and $RhCeO_2$/C also present the reflections corresponding to the fcc unit cell of rhodium metal.

The average crystallite size of CeO_2 and Rh^0 were estimated using the Scherrer's equation, and the results obtained are included in Table 1. The average crystallite size of ceria in the samples CeO_2/C and $RhCeO_2$/C is almost equal (3.8 and 3.6 nm, respectively). Thus, the thermal treatment performed after rhodium nitrate impregnation to CeO_2/C did not affect the crystallite size of ceria, which *a priori* was not obvious since a certain sintering could be expected. The crystallite size of CeO_2 obtained in the current study was smaller than values reported for pure ceria prepared by 500 °C-calcination of cerium nitrate (14 nm) [31], and this could be due to the dispersion of ceria on the carbon black surface. On the contrary, the crystallite size of Rh^0 was smaller on $RhCeO_2$/C (5.0 nm) than on Rh/C (11.8 nm), and strongly suggests that ceria favors the dispersion of rhodium and the formation of smaller crystallites. This observation is consistent with the fact that CeO_2-based oxides were incorporated successfully to the three-way catalysts formulations used for gasoline vehicles exhaust after-treatment in order to improve noble metal dispersion, among other benefits that were mentioned in Section 1 [15].

3.2.2. TEM

Fig. 6 shows TEM pictures of the powder catalysts CeO_2/C (Fig. 6a), Rh/C (Fig. 6b) and $RhCeO_2$/C (Fig. 6c), and these pictures support the XRD conclusions.

In Fig. 6b, the dark particles of rhodium are clearly distinguished from the carbon support, the latter with the typical carbon black spherical shape. The EDS analysis confirmed that the dark particles are composed of rhodium. The size of most rhodium particles in the sample Rh/C is around 10 nm, which is quite in agreement with the XRD estimation.

In Fig. 6a, CeO_2 aggregates (black areas) are observed, and in the sample $RhCeO_2$/C (Fig. 6c), rhodium and CeO_2 cannot be distinguished to each other. The EDS analysis confirmed that the black spots observed in Fig. 6c contain both cerium and rhodium, and these species appear spread on the carbon surface. The size of these black spots is lower than 10 nm, supporting the hypothesis that CeO_2 improves the dispersion of rhodium.

3.2.3. XPS

The surface composition of the Rh/C and $RhCeO_2$/C samples as determined by XPS is included in Table 2. Carbon, oxygen and rhodium are detected in both catalysts, and cerium only appears

Table 1
Crystallite sizes determined by Scherrer's equation.

Catalyst	CeO_2 (nm)	Rh^0 (nm)
Rh/C	–	11.8
$RhCeO_2$/C	3.6	5.0
CeO_2/C	3.8	–

Table 2
Surface composition of the catalyst powders determined by XPS.

Catalyst	C (wt%)	O (wt%)	Rh (wt%)	Ce (wt%)
Rh/C	89.0	5.5	5.5	–
$RhCeO_2$/C	80.9	6.0	6.4	6.7

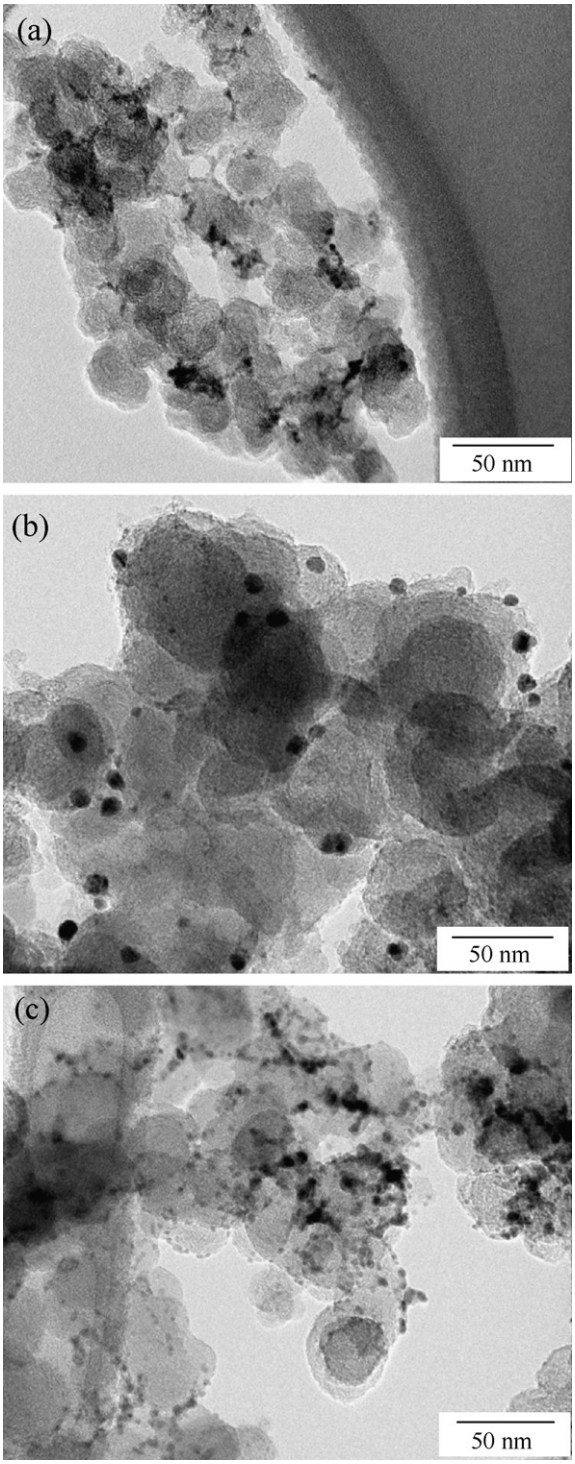

Fig. 6. TEM characterization of the catalyst powders. (a) CeO_2/C, (b) Rh/C, and (c) $RhCeO_2$/C.

in the catalyst $RhCeO_2$/C, as expected. The surface concentration of rhodium is higher in $RhCeO_2$/C than in Rh/C, which supports that CeO_2 promotes the dispersion of rhodium.

The Rh 3d photoelectron spectra of powder catalysts were analysed and are included in Fig. 7. The Rh $3d_{5/2}$ peak has been reported to appear at 307.0–307.5 eV [32–34] for Rh^0, at about 308.1 eV for Rh(I) [34], and at 308.3–310.5 eV for Rh(III) [32,34]. In addition, another band appears at higher binding energies attributed to the Rh $3d_{3/2}$ transition. The Rh $3d_{5/2}$ band of the catalysts Rh/C and

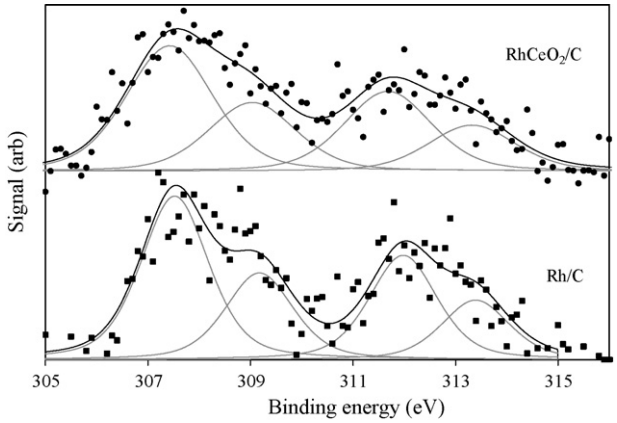

Fig. 7. Rh 3d photoelectron spectra of the catalyst powders.

$RhCeO_2$/C presents contribution of both $Rh^{\delta+}$ (B.E. = 308.9 eV) and Rh^0 (B.E. = 307.4 eV). The percentage of $Rh^{\delta+}$ and Rh^0 were calculated from the area of the deconvoluted peaks, and the results obtained are compiled in the Table 3. Both catalysts present higher proportion of Rh^0 (64.5–65.0%) than of $Rh^{\delta+}$ (35.5–35.0%), and the results obtained for Rh/C and $RhCeO_2$/C are very similar to each other.

On the other hand, the Ce 3d core level has been also analysed and the percentage of Ce^{3+} and Ce^{4+} on the powder sample $RhCeO_2$/C was calculated after deconvolution of the experimental spectra (not shown for brevity), from the ratio of the sum of the intensities of the u^0, u', v^0, and v' bands to the sum of the intensities of all the bands [35]. The Ce^{3+} percentage obtained (41.6%) is higher than that usually encountered in pure CeO_2 prepared by nitrate decomposition in air, where around 30% of cerium is Ce^{3+} [36], that is, the presence of carbon and the absence of O_2 during the thermal treatment favour the partial reduction of cerium.

3.2.4. TG-MS

In Fig. 8, the results obtained by TG-MS analysis are included. The weight lost by the bare carbon (sample C) is minor, as observed in Fig. 8a. From Fig. 8b it is deduced that few H_2O releases below 300 °C and CO/CO_2 emission at higher temperature is very low due to the little amount of surface oxygen complexes present in this commercial carbon black. The sample CeO_2/C releases more CO and CO_2 than the bare carbon, with the consequent higher weight loss. Carbon dioxide could come from CO_2 adsorbed on CeO_2 and also from surface oxygen complexes created on the carbon support during the decomposition of the cerium nitrate. This oxidation of the carbon surface is reasonable since $Ce(NO_3)_3{\cdot}6H_2O$ decomposition yields highly oxidizing nitrogen oxides.

The oxidation of the carbon support is much more important during the rhodium loading, and the weight loss of Rh/C and $RhCeO_2$/C observed in Fig. 8a is highest. The highest weight lost by the rhodium-containing samples is consistent to the higher release of CO and CO_2 (Fig. 8b) in comparison to the rhodium-free samples.

These TG-MS results are in agreement with the previous XPS characterization. The carbon support reacts with the rhodium species (nitrate and/or oxide) during the thermal treatment performed in inert atmosphere for the decomposition of rhodium

Table 3
Oxidation states of Ce and Rh in catalyst powders determined by XPS.

Catalyst	Ce^{3+} (%)	Ce^{4+} (%)	$Rh^{\delta+}$ (%) (B.E. = 307.4 eV)	Rh^0 (%) (B.E. = 308.9 eV)
Rh/C	–	–	35.0	65.0
$RhCeO_2$/C	41.6	58.4	35.5	64.5

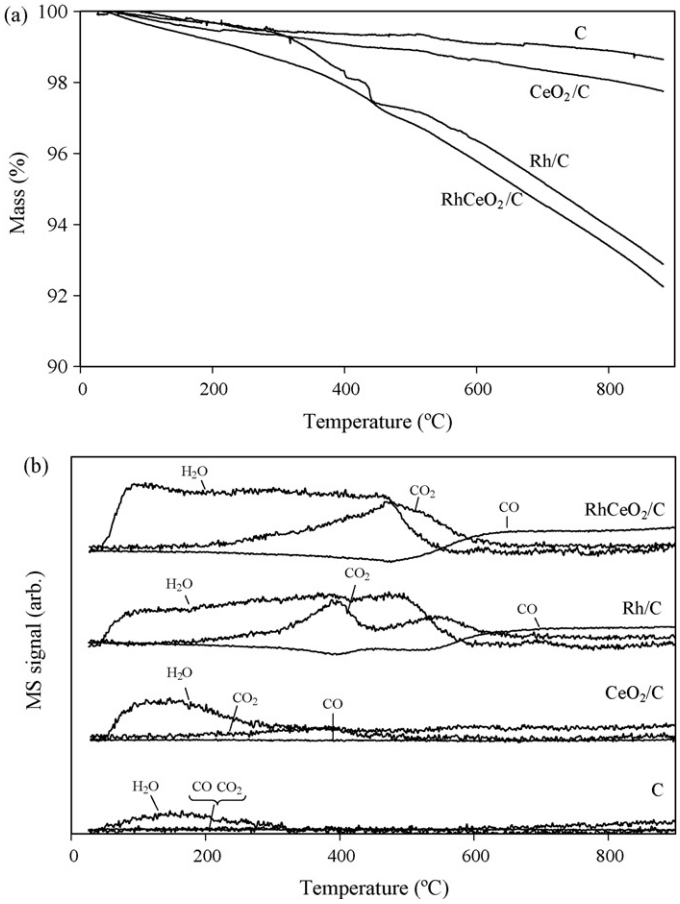

Fig. 8. TG-MS characterization of the catalyst powders. (a) Mass of sample and (b) MS signals.

nitrate. As a consequence of this rhodium nitrate/oxide–carbon reaction, rhodium is partially reduced, as observed by XPS, and the surface of the carbon support is partially oxidised, as deduced from TG-MS experiments.

3.2.5. H_2-TPR

Complementary information is obtained by H_2-TPR, and the TCD signal profiles are included in Fig. 9. The TCD signal of the bare carbon (sample C) rises slightly above 600 °C, and this is consistent with the reduction (or decomposition) of the little amount of surface oxygen complexes on this sample.

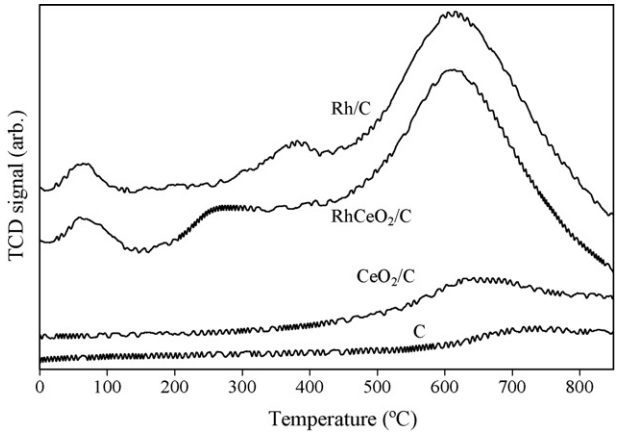

Fig. 9. H_2-TPR characterization of the catalyst powders.

The H_2-TPR profile of the sample CeO_2/C presents some differences regarding what one could expect for a pure CeO_2 sample. The H_2 consumption profile of pure CeO_2 usually presents two peaks around 425 and 800 °C due to surface and bulk ceria reduction, respectively [37]. This is not the shape of the profile obtained with the sample CeO_2/C, but a single band around 650 °C has been obtained. This atypical shape is consistent with the fact that cerium has been partially reduced by the carbon support during the sample preparation, and hence, part of cerium does not consume H_2 since is already in the Ce^{3+} oxidation state. Additionally, the reduction (or decomposition) of the surface oxygen groups on the carbon support will also contribute to the TCD signal.

The H_2-consumption profiles of Rh/C and $RhCeO_2$/C are complicated and several H_2-consuming phenomena can be inferred. The highest TCD signal level is reached around 625 °C in both cases, and this signal is consistent with the reduction (or decomposition) of the high amount of surface oxygen complexes created on the carbon support upon rhodium nitrate decomposition. The shoulders appearing at lower temperature could be attributed to the presence surface oxygen groups with different reducibility and stability. In the case of the catalyst $RhCeO_2$/C, the reduction of CeO_2 will also contribute to the TCD signal above 200 °C, and it must be taken into account that rhodium catalyses this process and shifts the CeO_2 reduction profile to lower temperature.

Rhodium oxide is reduced below 100 °C and a peak is clearly observed around this temperature in the profiles of both Rh/C and $RhCeO_2$/C catalysts. The number of moles of H_2 consumed in this low-temperature peak has been calculated, and the results are similar for both catalysts. It has been estimated that about 10% of the total rhodium loaded on the samples is reduced in the process responsible of this peak. For these calculations, it has been considered the reaction:

$$Rh_2O_3 + 3H_2 \rightarrow 2Rh + 3H_2O$$

This means that 90% of the total rhodium becomes Rh^0 during the preparation of the samples, and there are not appreciable differences in the oxidation state of rhodium between Rh/C and $RhCeO_2$/C. The results obtained by H_2-TPR predict a higher proportion of Rh^0 than those estimated by XPS (about 65%), which means that the oxidation of the rhodium particles mainly occurs on the surface. A tentative explanation is that rhodium is completely reduced by the carbon support during the thermal treatment performed for rhodium nitrate decomposition, and the surface of the rhodium particles is partially oxidized afterwards once the catalysts are exposed to the atmosphere.

3.2.6. XAS

The XANES region for the both, Rh/C and $RhCeO_2$/C along with rhodium foil are shown in Fig. 10. The XANES region for both the catalyst samples (Rh/C and $RhCeO_2$/C) are very similar and have virtually the same edge energy (23211.71 eV) indicating that the oxidation state of the rhodium is the same in both samples, in accordance with H_2-TPR and XPS conclusions. The white line intensity is however, larger for both samples when compared to the rhodium foil and can be attributed to oxidation due to exposure to air.

The extent of oxidation appears to be identical for both samples, as seen in the Fourier-transformed data in *r*-space, shown in Fig. 11 where it is discussed in greater detail. In the Fourier-transformed data, the peaks at different distances correspond to the various atoms neighboring the scattering rhodium atom. The broad peak centered at ca. 1.8 Å is due to Rh–O scattering and the peak at ca. 2.5 Å is due to Rh–Rh scattering. Note that the peaks are shifted to lower values of radius when compared to the actual bond distances. This is generally seen in the visual representation of the Fourier-transformed data and is a consequence of the phase-shift

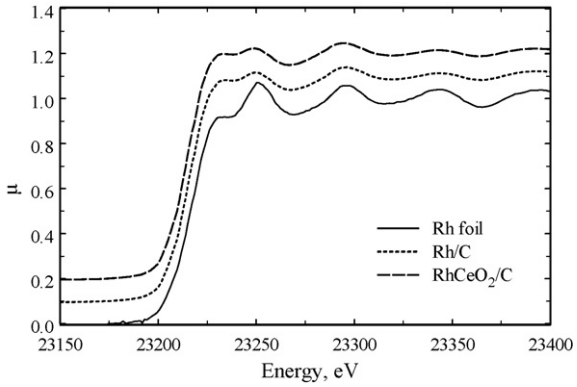

Fig. 10. XANES region for Rh/C, $RhCeO_2$/C and Rh foil.

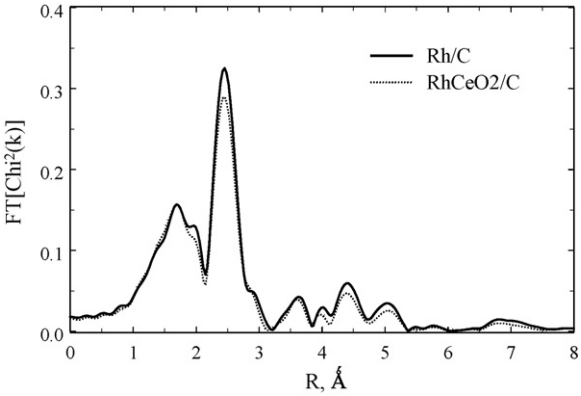

Fig. 11. Pseudo-radial distribution function obtained from the Fourier transformed data in r-space.

Table 4
EXAFS fit results for Rh/C and $RhCeO_2$/C. The uncertainties obtained are indicated in parentheses.

Sample	N_{Rh-Rh}	ΔE (eV)	ΔR (Å)	σ^2 (Å^2)
Rh/C	6.1 (0.4)	2.3 (1)	−0.008 (5)	0.004
$RhCeO_2$/C	5.4 (0.4)	1.2 (1)	−0.010 (6)	0.004

term in the EXAFS equation. The actual bond distances are obtained from the fit results and are shown along with the rest of the fit parameters in Table 4. The data collected was of excellent quality and displayed no significant noise levels even until k values of 16 Å^{-1}. The data in k-space is shown in Fig. 12. Since the particle size is obtained chiefly from determining the first-shell coordination

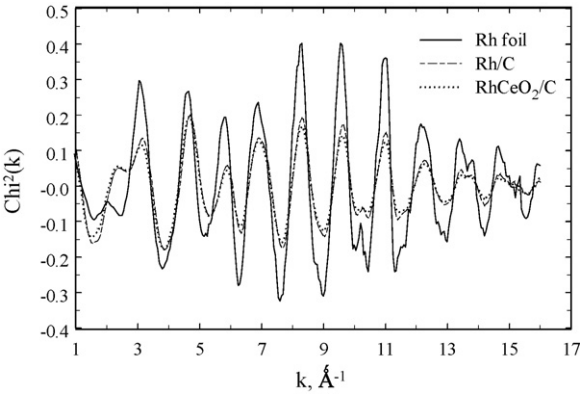

Fig. 12. Samples and Rh foil data as seen in k-space.

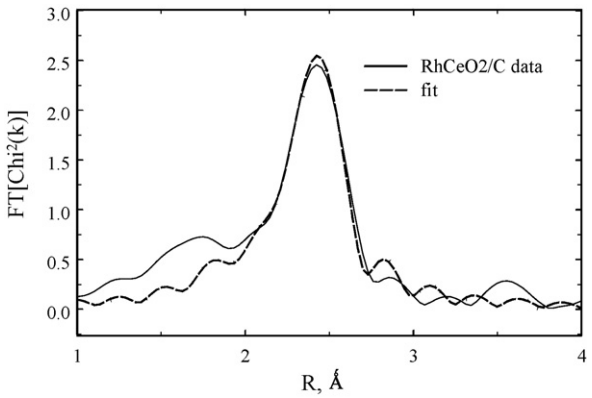

Fig. 13. Experimental data and representative fit using only Rh–Rh path for $RhCeO_2$/C sample.

number around rhodium, only the main Rh–Rh backscattering peak of the experimental data from both samples were fit and analyzed.

The data from both samples and foil were fit allowing all four parameters (amplitude, ΔE, ΔR and σ^2) to vary. Here, the amplitude is the intensity of scattering, ΔE is change in the edge energy from the standard value of the Rh K-edge, ΔR is the change in bond distance and σ^2 is the Debye–Waller factor representative of the total extent of disorder in the samples. The many body amplitude reduction factor (S_0^2) parameter for rhodium is calculated to be 0.921 using FEFF 8.0. The coordination numbers (N_{Rh-Rh}) are typically obtained using the amplitudes and the S_0^2 value for the scattering atom. Since the value of σ^2 is highly correlated with the amplitudes, the fits were carried out for a second time using only one representative value of σ^2 in order to make the comparisons of N_{Rh-Rh} between the samples more meaningful. The results of the fit for $RhCeO_2$/C are shown in Fig. 13.

The coordination numbers from the fit results clearly indicate that the particles in the rhodium supported on CeO_2/C are smaller than the carbon supported rhodium. The bond distance of the Rh–Rh path obtained from the fit is 2.686 Å and is comparable to the Rh–Rh distance in the foil. These findings are entirely consistent with TEM, XRD and XPS results and suggest that the rhodium in the $RhCeO_2$/C catalyst sample is in the same oxidation state but is dispersed to a larger extent when compared with the Rh/C catalyst sample.

In conclusion, the promoting effect of ceria in the electrocatalytic activity of rhodium seems to be related to the improved rhodium dispersion. This effect contrasts with the effect attributed to ceria on Pd and Pt activity. The promoting effect of CeO_2 to Pd and Pt towards electro-oxidation of ethanol has been ascribed to both a bifunctional-effect (promoted mechanism) and an electronic effect (intrinsic mechanism) [12,38,39]. The bi-functional mechanism involves supplying oxygen atoms at an adjacent site of promoting elements such as Ru and CeO_2 at lower potentials than that accomplished by Pt. Thus, CO or other oxide species strongly adsorbed on Pt are easily oxidized to CO_2. The promoter effect may also lie in an electronic effect (intrinsic mechanism) by modifying the electronic structure of Pt and lowering the potential of fuels adsorption.

4. Conclusions

In this study, the effect of ceria in the electrocatalytic activity of rhodium for ethanol electro-oxidation in alkali media has been studied, and the following can be concluded:

- The onset potential of oxidation on $RhCeO_2$/C was shifted negatively as compared to that on Rh/C, indicating better activity

of the former catalyst. However, the active sites are believed to be located only on rhodium since ceria itself does not show any catalytic activity towards oxidation of ethanol.

- The promoting effect of ceria seems to be related to the improved rhodium dispersion, as confirmed by XRD, TEM, XPS and EXAFS, and there were not found appreciable differences (by H_2-TPR, XPS and XANES) in the oxidation state of rhodium between Rh/C and $RhCeO_2$/C.
- The carbon support reacts with rhodium (both in Rh/C and $RhCeO_2$/C) during the thermal treatment performed in inert atmosphere for the decomposition of rhodium nitrate, and rhodium species are reduced to Rh^0 while the surface of the carbon support is oxidised. The rhodium particles surface seems to be oxidized once the catalysts are exposed to the atmosphere.
- The carbon support also reacts with the cerium precursor during the thermal treatment performed in inert atmosphere for the decomposition of cerium nitrate. As a consequence of this reaction, ceria on the catalyst $RhCeO_2$/C is only partially oxidized and the carbon surface is covered with oxygen complexes.

Acknowledgment

The authors thank the financial support of the Spanish Ministry of Education and Science by funding the project MAT2006-12635.

References

[1] E. Antolini, Journal of Power Sources 170 (2007) 1–12.
[2] Y. Bai, J. Wu, X. Qiu, J. Xi, J. Wang, J. Li, W. Zhu, L. Chen, Applied Catalysis B: Environmental 73 (2007) 144–149.
[3] A. Kowal, Nature Materials 8 (2009) 325–330.
[4] C.J. Houtman, M.A. Barteau, Journal of Catalysis 130 (2) (1991) 528–546.
[5] K. Bergamaski, J.F. Gomes, B.E. Goi, F.C. Nart, Eclética Química 28 (2) (2003) 87–92.
[6] F.H.B. Lima, E.R. Gonzalez, Electrochimica Acta 53 (2008) 2963–2971.
[7] J.P.I. de Souza, S.L. Queiroz, K. Bergamaski, E.R. Gonzalez, F.C. Nart, Journal Physical Chemistry B 106 (2002) 9825–9830.
[8] L. Jiang, L. Colmenares, Z. Jusys, G.Q. Sun, R.J. Behm, Electrochimica Acta 53 (2007) 377–389.
[9] P. Bommersbach, M. Mohamedi, D. Guay, Journal of The Electrochemical Society 154 (8) (2007) B876–B882.
[10] J. Liu, J. Ye, C. Xu, S. Jiang, Y. Tong, Electrochemistry Communications 9 (2007) 2334–2339.
[11] C. Xu, P. Shen, Y. Liu, Journal of Power Sources 164 (2007) 527–531.
[12] P. Shen, C. Xu, Electrochemistry Communications 8 (2006) 184–188.
[13] J. Mann, N. Yao, A.B. Bocarsly, Langmuir 22 (2006) 10432–10436.
[14] C. Xu, Z. Tian, P. Shen, S.P. Jiang, Electrochimica Acta 53 (2008) 2610–2618.
[15] J. Kaspar, P. Fornasiero, M. Graziani, Catalysis Today 50 (1999) 285–298.
[16] H.S. Gandhi, G.W. Graham, R.W. McCabe, Journal of Catalysis 216 (2003) 433–442.
[17] M.V. Twigg, Applied Catalysis B: Environmental 70 (2007) 2–15.
[18] M. Pourbaix, Atlas of Electrochemical Equilibria in Aqueous Solutions, Pergamon Press, 1966.
[19] H. Wang, Z. Jusys, R.J. Behm, Journal of Power Sources 154 (2006) 351–359.
[20] R.T.S. Oliveira, M.C. Santos, B.G. Marcussi, S.T. Tanimoto, L.O.S. Bulhões, E.C. Pereira, Journal of Power Sources 157 (2006) 212–216.
[21] E. Vesselli, A. Baraldi, G. Comelli, S. Lizzit, R. Rosei, ChemPhysChem 5 (2004) 1133–1140.
[22] J.M. Ziegelbauer, D. Gatewood, D.E. Ramaker, A.F. Gullá, M.J.-F. Guineld, F. Erns, S. Mukerjeea, Fundamental investigation of the oxygen reduction reaction on rhodium sulfide-based chalcogens, in preparation.
[23] Q. He, W. Chen, S. Mukerjee, S. Chen, F. Laufek, Journal of Power Sources 187 (2009) 298–304.
[24] S.A. Kirillov, P.E. Tsiakaras, I.V. Romanova, Journal of Molecular Structure 651–653 (2003) 365–370.
[25] T. Maiyalagan, Journal of Power Sources 179 (2008) 443–450.
[26] A.L. Santos, D. Profeti, P. Olivi, Electrochimica Acta 50 (2005) 2615–2621.
[27] D. Profeti, P. Olivi, Electrochimica Acta 49 (2004) 4979–4985.
[28] D. Terribile, A. Trovarelli, J. Llorca, C. de Leitenburg, G. Dolcetti, Catalysis Today 43 (1998) 79.
[29] G. Suna, X. Li, H. Yan, J. Qiu, Y. Zhang, Carbon 46 (2008) 476–481.
[30] A.E. Nelson, K.H. Schulz, Applied Surface Science 210 (2003) 206–221.
[31] I. Atribak, A. Bueno-López, A. García-García, Journal of Catalysis 259 (2008) 123–132.
[32] http://www.lasurface.com/ (access in August 2008).
[33] X.D. Wu, L.H. Xu, D. Weng, Applied Surface Science 221 (2004) 375.
[34] J. Soria, A. Martínez-Arias, J.L.G. Fierro, J.C. Conesa, Vacuum 46 (1995) 1201.
[35] A. Laachir, V. Perrichon, A. Badri, J. Lamotte, E. Catherine, J.C. Lavalley, J. El Fallal, L. Hilaire, F. le Normand, E. Quéméré, G.N. Sauvion, O.J. Touret, Journal of the Chemical Society, Faraday Transactions 87 (1991) 1601.
[36] A. Bueno-López, I. Such-Basáñez, C. Salinas-Martínez de Lecea, Journal of Catalysis 244 (2006) 102–112.
[37] G.L. Markaryan, L.N. Ikryannikova, G.P. Muravieva, A.O. Turakulova, B.G. Kostyuk, E.V. Lunina, V.V. Lunin, E. Zhilinskaya, A. Aboukais, Colloids Surfaces A 151 (1991) 435.
[38] C. Xua, Z. Tian, P. Shen, S. Ping Jiang, Electrochimica Acta 53 (2008) 2610–2618.
[39] C. Xua, P. Shen, Y. Liu, Journal of Power Sources 164 (2007) 527–531.